Shear Instabilities in Metallic Nanoparticles: Hydrogen-Stabilized Structure of Pt$_{37}$ on Carbon

Lin-Lin Wang* and D. D. Johnson*

Contribution from the Department of Materials Science and Engineering, and the Frederick Seitz Materials Research Laboratory, University of Illinois, Urbana-Champaign, Illinois 61801

Received December 6, 2006; E-mail: llw@uiuc.edu; duanej@uiuc.edu

Abstract: Using density functional theory calculations, we have studied the morphology of a Pt$_{37}$ nanoparticle supported on carbon with and without hydrogen (H) passivation that arises with postprocessing of nanoparticles before characterization. Upon heating in an anneal cycle, we find that without H (e.g., in a helium atmosphere or evacuation at high temperature), the morphology change of a truncated cuboctahedral Pt$_{37}$ is driven by the shearing of (100) to (111) facets to lower the surface energy, a remnant shear instability that drives surface reconstruction in semi-infinite Pt(100). With H passivation from a postprocessing anneal, we show that the sheared structure automatically reverts to the observed truncated cuboctahedral structure and the average first nearest-neighbor Pt−Pt bond length increases by 3%, agreeing well with experiment. We explain the stabilization of the truncated cuboctahedral structure due to H passivation via adsorption energetics of hydrogen on Pt(100) and (111) facets, specifically, the preference for H adsorption at bridge sites on (100) facets, which should be considered in a realistic model for H adsorption on Pt nanoparticles. We find that dramatic morphological change of a nanoparticle can occur even with small changes to first-shell Pt−Pt coordination number. The implications of our findings when comparing to experimental data are discussed.

Introduction

Supported metal nanoparticles play a major role in many important physical and chemical processes such as heterogeneous catalysis. The microstructure and morphology of supported metal nanoparticles largely determine the reactivity and selectivity. Considerable effort has been expended to characterize experimentally the morphology of supported metal nanoparticles. Using chemical vapor deposition (CVD) and scanning tunneling microscopy (STM), Pt deposition on graphite has been studied previously.[1−3] Given the rather weak interaction between Pt and C, the samples consist mostly of 3-dimenional Pt islands,[2] although, surprisingly, a monolayer of Pt has been found on graphite.[2] Using metallorganics as precursor, our collaborators have synthesized Pt and Pt−Ru nanoparticles on high-area carbon with very narrow size distributions (a few nanometers in diameter) for catalysis use.[4−10] Detailed structural models of

these nanoparticles were deduced from data obtained from *in situ* extended X-ray absorption fine structure spectroscopy (EXAFS), scanning transmission electron microscopy (STEM), microprobe energy-dispersive X-ray analysis (EDX), and electron microdiffraction. The previous study[7] showed that the Pt nanoparticles obtained from metallorganic precursor and reduced by hydrogen (H$_2$) at high temperature are exceptionally well-defined materials with a truncated cuboctahedral (TC) structure based upon a face-centered-cubic, close-packed structure.

Recently, using TC Pt$_{37}$ and Pt$_6$Ru$_{31}$ clusters supported on graphene (a model for the carbon support), we applied density functional theory (DFT) to calculate the properties, including bond-length distributions, and we showed that the large Pt−Pt bond-length disorder was intrinsic to the support/metal-nanoparticle system,[11] a result of symmetry change and cluster-support interactions. However, when synthesizing metal nanoparticles from metallorganics, it is a common practice to postanneal the nanoparticles (approximately 700 K for Pt nanoparticles on carbon[7]) to remove any leftover organics, then, prior to characterization, the particles are cooled in H$_2$-rich environment to room temperature to prevent oxidation. In contrast, helium (He) can also be used to prevent oxidation of nanoparticles at room temperature. The adsorbed H can be removed by evacuation at high temperature. Different postprocessing of the nanoparticles before characterization has a

(1) Muller, U.; Sattler, K.; Xhie, J.; Venkateswaran, N.; Raina, G. *J. Vac. Sci. Technol., B* **1991**, *9*, 829−832.
(2) Clark, G. W.; Kesmodel, L. L. *J. Vac. Sci. Technol., B* **1993**, *11*, 131−136.
(3) Atamny, F.; Burgi, T.; Schlogl, R.; Baiker, A. *Surf. Sci.* **2001**, *475*, 140−148.
(4) Nashner, M. S.; Frenkel, A. I.; Adler, D. L.; Shapley, J. R.; Nuzzo, R. G. *J. Am. Chem. Soc.* **1997**, *119*, 7760−7771.
(5) Nashner, M. S.; Frenkel, A. I.; Somerville, D.; Hills, C. W.; Shapley, J. R.; Nuzzo, R. G. *J. Am. Chem. Soc.* **1998**, *120*, 8093−8101.
(6) Hills, C. W.; Nashner, M. S.; Frenkel, A. I.; Shapley, J. R.; Nuzzo, R. G. *Langmuir* **1999**, *15*, 690−700.
(7) Frenkel, A. I.; Hills, C. W.; Nuzzo, R. G. *J. Phys. Chem. B* **2001**, *105*, 12689−12703.
(8) Hills, C. W.; Mack, N. H.; Nuzzo, R. G. *J. Phys. Chem. B* **2003**, *107*, 2626−2636.
(9) Maillard, F.; Schreier, S.; Hanzlik, M.; Savinova, E. R.; Weinkauf, S.; Stimming, U. *Phys. Chem. Chem. Phys.* **2005**, *7*, 385−393.

(10) Teliska, M.; O'Grady, W. E.; Ramaker, D. E. *J. Phys. Chem. B* **2004**, *108*, 2333−2344.
(11) Wang, L. L.; Khare, S. V.; Chirita, V.; Johnson, D. D.; Rockett, A. A.; Frenkel, A. I.; Mack, N. H.; Nuzzo, R. G. *J. Am. Chem. Soc.* **2006**, *128*, 131−142.

profound effect on the structures assessed. We note that several studies have shown that the adsorption of small molecules, such as H_2, CO, and O_2, can induce structural changes of semi-infinite Pt surfaces.[12,13] A recent STEM experiment by Hansen et al.[14] on Cu nanoparticles (4 nm diameter) supported on ZnO showed that small adsorbates also could induce morphological change in metal nanoparticles.

For the adsorption of hydrogen on Pt nanoparticles, three kinds of effects have been studied so far. First, the H-induced changes in the Pt $L_{2,3}$ white lines in X-ray absorption have been studied by both X-ray absorption near edge spectroscopy (XANES) experiment[15−18] and theoretical calculations.[19] Second, there is an increased Pt−Pt first nearest-neighbor (NN) bond length in the Pt nanoparticles with the first shell coordination number between 5 and 7 induced by H adsorption on various supports, as reported in many EXAFS experiments.[16,20−24] Third, the H adsorption site and strength is both support ionicity and coverage dependent, suggested in a recently proposed three-site model.[21,22,25] Depending on the coverage, H can be weakly as well as strongly bonded.

In this article, we concentrate on the morphology change of the Pt nanoparticles supported on carbon due to the postprocessing effects with and without H passivation. We address a range of important questions, including: Is there a shear instability of the supported Pt nanoparticles? Does H passivation induce structural stability? And how much increase is in Pt−Pt first nearest-neighbor bond length due to H passivation? The answers to these questions are critical to interpret and/or predict the experimental observations.

To detail and explain the effects of postanneal with He or H_2 atmospheres on the nanoparticles morphology, we use DFT to study the structural behavior of a well-characterized Pt_{37} supported on graphene (Pt_{37}/C) without and with H passivation. We find that without H passivation the TC structure has a shear instability—reminiscent of Pt(001) surface reconstruction—such that the Pt(001) facets shear to a Pt(111)-like facet to lower its energy.[12] With H passivation, we show that this sheared structure automatically reverts back to the TC. Moreover, the average first nearest-neighbor Pt−Pt bond length increases by 3%, which agrees quantitatively with experiments.[16,20−24] We explain the stabilization of TC structure by H passivation with the adsorption

energetics of H_2 on Pt(100) and (111) facets. In addition, we discuss the implication of our results to the H adsorption model on Pt nanoparticles and the relation between first-shell coordination number and morphology change.

The paper is organized beginning with a section on computational details, followed by the results and comparison to experiment for (un)passivated nanoparticles and their morphological changes and stabilization, and final concluding remarks. Importantly, so as not to repeat unnecessarily, we utilize the analysis of Pt nanoparticle bond lengths and distributions detailed in our recent joint theoretical and experimental paper.[11]

Computational Details

For the electronic-structure calculation, we use DFT[26−28] within the local density approximation (LDA) based upon the exchange-correlation (XC) functional constructed by Ceperley-Alder[29] and parametrized by Perdew and Zunger.[30] We utilized a plane-wave basis set as implemented in the Vienna Atomic Simulation Package (VASP)[31−34] within the projected augmented wave (PAW) method.[35,36] A kinetic energy cutoff of 250 eV in the plane-wave basis set was tested for convergence and found sufficient.

Calculations for the supported systems were done in a 7×7 graphene hexagonal supercell of $17.15 \times 17.15 \times 19.92$ Å^3 with periodic boundary conditions. Sufficient surrounding vacuum (at least 12 Å) is included to avoid unphysical interactions among repeating slabs in the z direction. Separate calculations verified that the use of a single graphite sheet as an approximation for the support did not affect the results while markedly reducing the computational cost. We find that the k-point mesh of $1 \times 1 \times 1$ is sufficient to give reliable results. The total energy is converged to 3 meV/atom and the system is relaxed fully until the absolute force on each atom is smaller than 0.02 eV/Å. In our first-principles molecular dynamics (MD) simulations to anneal the system and to reduce markedly the computational cost, we use the time step of 20 femtosecond. We can use such a large time step only by setting that the mass of C in graphene support to be 10 times larger than that of Pt. The goal of utilizing this approach within the initial simulations is to make the Pt cluster sample large configuration changes with long enough simulation time in the presence of the graphene support. The details of the phonon modes in the graphene are smeared out. For the calculations of H_2 adsorption on Pt (111) and (100) surfaces, four atomic layer slabs are used with the bottom two layers fixed at the bulk value. When considering different coverage of H, 1×1 and 2×2 surface unit cells are used with $24 \times 24 \times 1$ and $12 \times 12 \times 1$ k-point meshes, respectively.

Finally, to validate subsequent structural comparisons, we note the VASP-PAW method reproduces (within the expected 0.5−2.0% error for LDA) the elemental lattice constants of fcc Pt (3.91 Å) and hexagonal graphite (2.45, 6.69 Å), which compares well with the observed values of 3.92 Å[37] and 2.46, 6.71 Å,[38] respectively. Clearly,

(12) Hu, X. M.; Lin, Z. D. *Phys. Rev. B: Condens. Matter Mater. Phys.* **1995**, *52*, 11467−11470.
(13) Somorjai, G. A.; Hwang, K. S.; Parker, J. S. *Top. Catal.* **2003**, *26*, 87−99.
(14) Hansen, P. L.; Wagner, J. B.; Helveg, S.; Rostrup-Nielsen, J. R.; Clausen, B. S.; Topsoe, H. *Science* **2002**, *295*, 2053−2055.
(15) Vaarkamp, M.; Miller, J. T.; Modica, F. S.; Koningsberger, D. C. *J. Catal.* **1996**, *163*, 294−305.
(16) Reifsnyder, S. N.; Otten, M. M.; Sayers, D. E.; Lamb, H. H. *J. Phys. Chem. B* **1997**, *101*, 4972−4977.
(17) Asakura, K.; Chun, W. J.; Shirai, M.; Tomishige, K.; Iwasawa, Y. *J. Phys. Chem. B* **1997**, *101*, 5549−5556.
(18) Ramaker, D. E.; Mojet, B. L.; Oostenbrink, M. T. G.; Miller, J. T.; Koningsberger, D. C. *Phys. Chem. Chem. Phys.* **1999**, *1*, 2293−2302.
(19) Ankudinov, A. L.; Rehr, J. J.; Low, J.; Bare, S. R. *Phys. Rev. Lett.* **2001**, *86*, 1642−1645.
(20) Alexeev, O. S.; Li, F.; Amiridis, M. D.; Gates, B. C. *J. Phys. Chem. B* **2005**, *109*, 2338−2349.
(21) Oudenhuijzen, M. K.; Bitter, J. H.; Koningsberger, D. C. *J. Phys. Chem. B* **2001**, *105*, 4616−4622.
(22) Oudenhuijzen, M. K.; van Bokhoven, J. A.; Miller, J. T.; Ramaker, D. E.; Koningsberger, D. C. *J. Am. Chem. Soc.* **2005**, *127*, 1530−1540.
(23) Zhang, Y. H.; Toebes, M. L.; van der Eerden, A.; O'Grady, W. E.; de Jong, K. P.; Koningsberger, D. C. *J. Phys. Chem. B* **2004**, *108*, 18509−18519.
(24) Kang, J. H.; Menard, L. D.; Nuzzo, R. G.; Frenkel, A. I. *J. Am. Chem. Soc.* **2006**, *128*, 12068−12069.
(25) Oudenhuijzen, M. K.; van Bokhoven, J. A.; Ramaker, D. E.; Koningsberger, D. C. *J. Phys. Chem. B* **2004**, *108*, 20247−20254.

(26) Hohenberg, P.; Kohn, W. *Phys. Rev. B: Condens. Matter Mater. Phys.* **1964**, *136*, B864−&.
(27) Kohn, W.; Sham, L. J. *Phys. Rev.* **1965**, *140*, 1133−&.
(28) Dreizler, R. M.; Gross, E. K. U. *Density Functional Theory: An Approach to the Quantum Many-Body Problem*; Springer-Verlag: New York, 1990.
(29) Ceperley, D. M.; Alder, B. J. *Phys. Rev. Lett.* **1980**, *45*, 566−569.
(30) Perdew, J. P.; Zunger, A. *Phys. Rev. B: Condens. Matter Mater. Phys.* **1981**, *23*, 5048−5079.
(31) Kresse, G.; Technische Universität Wien, Ph.D. Thesis, 1993.
(32) Kresse, G.; Furthmüller, J. *Comput. Mater. Sci.* **1996**, *6*, 15−50.
(33) Kresse, G.; Furthmüller, J. *Phys. Rev. B: Condens. Matter Mater. Phys.* **1996**, *54*, 11169−11186.
(34) Kresse, G.; Hafner, J. *Phys. Rev. B: Condens. Matter Mater. Phys.* **1993**, *47*, 558−561.
(35) Blöchl, P. E. *Phys. Rev. B: Condens. Matter Mater. Phys.* **1994**, *50*, 17953−17979.
(36) Holzwarth, N. A. W.; Matthews, G. E.; Dunning, R. B.; Tackett, A. R.; Zeng, Y. *Phys. Rev. B: Condens. Matter Mater. Phys.* **1997**, *55*, 2005−2017.
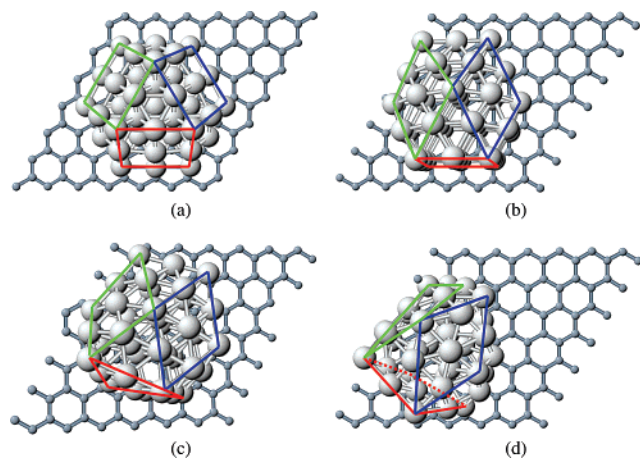(37) Kittel, C. *Introduction to Solid State Physics*, 7 ed.; Wiley: New York, 1996.

Figure 1. Morphological changes of a Pt_{37} cluster (no H passivation) on graphene. (a) Truncated cuboctahedral (TC) structure with three (100) facets highlighted in red, green, and blue. (b) Structure is derived from (a) by shearing of two of the (100) facets, green and blue, to (111) facets. (c) Structure is derived from (b) by shearing of the last (100) facet, red, to (111) facet. (d) Structure is derived from (c) by additional rearrangement of the Pt atoms. The total energy is lowered gradually from (a) to (d) as listed in Table 1. The large sphere stands for Pt and small for C.

Table 1. Relative Energy Reduction and Mean Interatomic Distance (MIAD) for the Shape Change of Pt_{37}/C (no H Passivation)

structure[a]	energy (eV)	MIAD (Å)
a	0.00	5.41
b	1.54	5.36
c	1.74	5.36
d	2.62	5.30

[a] See Figure 1 for the structures denoted by a−d.

we are within 0.5% error for the reference systems. We note for later that the lattice constant of bulk Pt gives a near-neighbor bond length of 2.765 Å.

Results and Discussion

Morphology Change of Pt_{37} on Graphene. The morphology change of a Pt_{37}/C is presented in Figure 1. We start with the TC structure as shown in Figure 1a, which consists of three close-packed atomic layers, with 19, 12, and 6 Pt atoms in the bottom, central, and top layers, respectively. The TC structure has three (111) and (100) facets. The three (100) facets are highlighted in Figure 1a in red, green, and blue. To find a lower energy structure, we heat up the system to 1000 K via a first-principle MD simulation and let the system to rearrange itself without any constraint. Then, several lowest potential energy structures are singled out with further ionic relaxation at 0 K to find their equilibrium. From this procedure, we have found several structures within a class that have lower energy than the TC structure. Three of such structures are shown in Figure 1b, c, and d, with the relative reduction in total energy listed in Table 1 with respect to the TC structure.

Although the structure in Figure 1d is not guaranteed to be the global minimum, the trend of morphology change from (a) to (d) is obvious. It is well-known that the (100) open surface of semi-infinite Pt is not stable; it relaxes to resemble (111) surface to lower its surface energy. For small Pt cluster with well-defined (100) facets like Pt_{37}, we find that this shear-
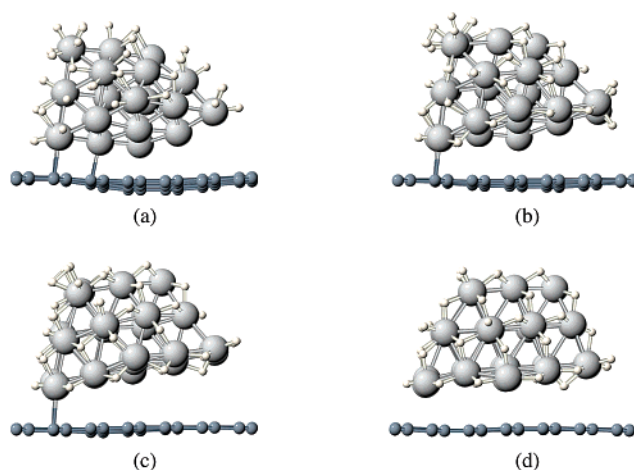

Figure 2. Snapshots of relaxation of 54 H atoms passivated Pt_{37}/C. From (a) to (d), the total energy is lowered by only ionic relaxation. Change from the structure of sheared TC (Figure 1b) to TC (Figure 1a) is barrier-free. Large, medium, and small spheres are Pt, C, and H atoms, respectively.

instability behavior remains. Comparing Figure 1b with a, the cluster is sheared such that two of the three (100) facets become (111) facets. The energy reduction is 1.54 eV. A further shear of the third (100) facet, as shown in Figure 1c, is not well adapted with the underlying graphene lattice, so the energy reduction is only about 0.2 eV with respect to Figure 1b, see Table 1. The increased Pt−Pt interaction by shearing is accompanied with decreased Pt−C interaction with long Pt−C distance. To become even lower in energy, shown in Figure 1d, Pt atoms in the bottom half of the cluster rearrange themselves to shorten distances from carbon and increase Pt−C interaction with respect to Figure 1b and c. As the result, some parts of the original and (100)-derived (111) facets are distorted, but the energy reduction of 0.9 eV with respect to Figure 1c is quite large.

As noted earlier, the driving force of the morphology change is the lowering of Pt cluster surface energy. To evaluate the influence of shearing on the overall Pt−Pt bonds, we use a Pt−Pt mean interatomic distance[39] (MIAD) of the cluster as $l_{MIAD} = N_{prs}^{-1} \sum_{n=1}^{N_{prs}} |\Delta R_n|$, where n runs over all pairs of Pt atoms in the cluster and ΔR_n is the distance between each of those pairs. This MIAD is listed in Table 1. As the total energy is lowered gradually from (a) to (d), the Pt−Pt MIAD decreases from 5.41 to 5.30 Å. Therefore, lowering of the total energy by morphology change is also the result of decreasing of Pt−Pt bond length, i.e., stronger Pt−Pt interactions.

Hydrogen-Passivated Pt_{37} on Graphene. To study the effect of hydrogen passivation on the morphology of Pt_{37}/C, we attach 54 H atoms to the Pt atoms on the outer surface of the sheared TC structure in Figure 1b, except for the interface region between the cluster and support. Figure 2 shows the snapshots of the ionic relaxation of the system. From Figure 2a−d, the shearing of the two (100) facets is gradually lifted and the (100) facets are restored to be that of the TC structure. The fact that just ionic relaxation is capable of causing the transformation shows that the transition is barrier-free (a downhill transition once H is adsorbed). A follow-up first-principle MD simulation at 1000 K for the TC structure of Figure 2d shows that the

(38) Yin, M. T.; Cohen, M. L. *Phys. Rev. B: Condens. Matter Mater. Phys.* **1984**, *29*, 6996−6998.

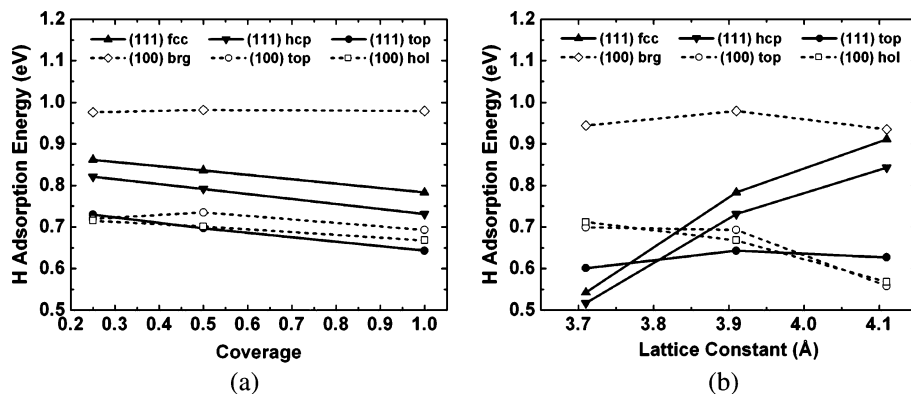(39) Kummel, S.; Akola, J.; Manninen, M. *Phys. Rev. Lett.* **2000**, *84*, 3827−3830.

Figure 3. Pt(111) and (100) hydrogen adsorption energy versus (a) coverage and (b) lattice constant at fixed coverage of 1.0. Results are given for fcc, hcp, and atop sites on Pt(111), as the bridge site is unstable, and bridge, atop, and hollow sites for Pt(100).

H-passivated TC is structurally very stable, for at this high temperature there is no change in symmetry, only variations caused by vibrational effects.

There are three features worth notice in Figure 2d. First, on the (100) and (111) facets, H atom prefers to adsorb on the bridge sites (along the bond between two Pt atoms) and hollow sites (within the triangle formed by three Pt surface atoms), respectively. Second, H appears underneath the cluster, i.e., in the interface region between the Pt_{37} cluster and carbon. This shows that the coverage of H on the outer surface is about the optimal. The appearance of H inside the interface region also agrees with a structural model recently proposed.[15,23] Third, the support has almost no buckling, in contrast to Figure 2a when the cluster is sheared (or equivalently, Figure 1b when no H is present). Thus, the Pt−C interaction is reduced significantly with the H passivation.

To explain the structural behaviors observed above on the H-passivated Pt_{37}/C. We studied the H_2 adsorption on semi-infinite Pt(111) and (100) surfaces. It is well-known that H_2 adsorbs dissociatively on Pt surface. In Figure 3a, the dependence of H adsorption energy on coverage on various adsorption sites on Pt(111) and (100) is shown. On Pt(111), we find that the dependence of adsorption energy on coverage is linear from 0.25 to 1. The lower coverage gives the larger adsorption energy. The preference of the adsorption sites does not change. An fcc site is the most preferred adsorption site, followed closely by an hcp site. Atop site is the least preferred site, whereas a bridge site is unstable and relaxes to fcc. The adsorption energy on a fcc site at 0.25 coverage is 0.86 eV. The preference and the adsorption energies agree well with earlier DFT studies.[40,41] On Pt(100), the dependence of adsorption energy on coverage is not linear, except for in the hollow site. For bridge and atop sites, the coverage of 0.5 gives the largest adsorption energy. The change of the adsorption energy with respect to coverage on Pt(100) is less than that on Pt(111). On Pt(100), the most preferred site is the bridge site. Atop and hollow sites are both the least preferred. The adsorption energy of 0.97 eV on the bridge site on Pt(100) is the largest among all the sites on both surfaces. The strong preference of H on the bridge site of transition metal (100) surface is not unusual, as a recent study showed that H prefers to adsorb on the bridge site on Ir(100) surface.[42]
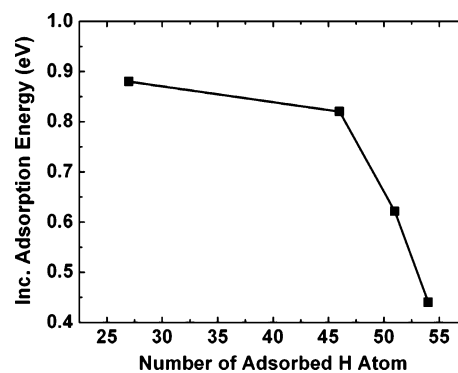
(40) Greeley, J.; Mavrikakis, M. *J. Phys. Chem. B* **2005**, *109*, 3460−3471.
(41) Papoian, G.; Norskov, J. K.; Hoffmann, R. *J. Am. Chem. Soc.* **2000**, *122*, 4129−4144.

Figure 4. Incremental adsorption energy of H on TC Pt_{37} supported on graphene.

Figure 3b shows the dependence of adsorption energy on lattice constant on various sites on both surfaces. For the bridge site on (100) and atop site on (111), the equilibrium lattice constant gives the largest adsorption energy and either contracting or expanding lattice constant by 5% lowers the adsorption energy. For the top and hollow sites on Pt(100), the smaller (larger) lattice constant gives larger (smaller) adsorption energy, and the expansion of lattice constant has larger effect than contraction on the adsorption energy. The opposite trend is true for the fcc and hcp sites on Pt(111). In a summary, because the lattice constant is contracted from the bulk value on the outer surface of a small Pt cluster, the adsorption of H atom on bridge sites on Pt(100) facet is preferred by at least 0.2 eV over 3-fold hollow sites on Pt(111) facet around 1.0 coverage. This explains very well the H configuration in the Pt_{37}/C passivated with 54 H in Figure 2. Most of H atoms adsorb on the bridge sites on Pt(100) facets and the 3-fold hollow sites on Pt(111) facets. Only very few H atoms adsorb on atop sites.

The TC−Pt_{37}/C has 27 Pt atoms on the outer surface. With all the bridge sites on (100) facets and 3-fold hollow sites on (111) facets occupied, the number of adsorbed H atom is 46. To get the optimal coverage of H on TC Pt_{37}/C, we calculated the adsorption energy of H on Pt_{37} passivated with 27, 46, 51, and 54 H atoms. The incremental adsorption energy per H atom is plotted in Figure 4. From 27 to 46 H, it shows that adding one more H causes a reduction of 0.8 eV in total energy until all the bridge and 3-fold hollow sites are filled. From 46 to 54 H, the energy reduction of adding one more H decreases

(42) Lerch, D.; Klein, A.; Schmidt, A.; Muller, S.; Hammer, L.; Heinz, K.; Weinert, M. *Phys. Rev. B: Condens. Matter Mater. Phys.* **2006**, *73*, 075430.
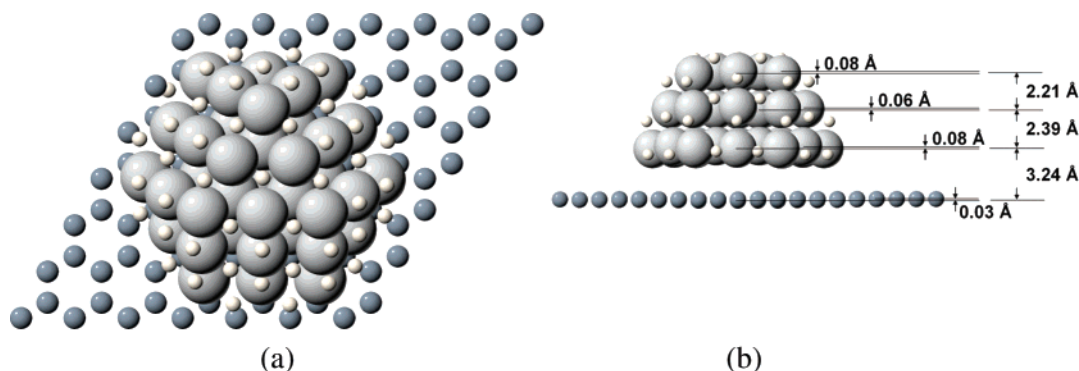
Figure 5. Structure of TC−Pt$_{37}$/C passivated with 46 H, (a) top and (b) side view (bonds not shown for clarity). Large, medium, and small spheres are Pt, C, and H, respectively.

precipitously from 0.8 to 0.4 eV on atop sites. Thus, the optimal coverage of TC−Pt$_{37}$/C is with 46 H atoms.

Recently, in their three-site adsorption model, Oudenhuijzen et al.[21,22,25] have shown that the atop site is preferred for H atom at low coverage on a small Pt$_4$ cluster, but the 2-fold edge and 3-fold hollow sites become preferred for H at high coverage. At even higher coverage, atop sites are occupied again, but with much less adsorption energy. Their findings that the most preferred adsorption sites are 2- and 3-fold sites for strongly bonded H at high coverage and the weakly bonded H occupies atop sites at even higher coverage agree with ours on a larger Pt cluster. However, unlike our calculations, they did not consider the adsorption of H on the (100) facets due to extreme small size of their cluster. Here, we show that under H$_2$ atmosphere, the open (100) facet in Pt nanoparticle actually can be stabilized by H passivation; thus, the adsorption sites on (100) facet should be strongly relevant to the experimental chemisorption data of H$_2$ in Pt nanoparticle catalyzed hydrogenolysis and hydrogenation reactions.

Properties of Pt$_{37}$/C Passivated by 46 H: Comparison to Experiment. Structure and Bond Length Distribution. The structure of TC−Pt$_{37}$/C optimally passivated with 46 H atoms is shown in Figure 5. As explained earlier, H atoms adsorb on bridge sites on (100) facet and on 3-fold hollow sites on (111) facet, as evidenced by H locations shown in Figure 5a. In Figure 5b, the intralayer buckling and interlayer distances are shown. Compared with those for the bare TC−Pt$_{37}$/C (details in ref 11), the intralayer buckling of 0.03 Å is very small, so the graphene sheet is undistorted by the presence of the H-passivated Pt cluster, and there is a large adsorption distance of 3.24 Å between Pt$_{37}$ and graphene that reflects the weak Pt−C interaction. In contrast to the bare Pt$_{37}$/C,[11] the intralayer buckling of the three Pt layers are all very small, in the range of 0.06 to 0.08 Å. As a result, there is a complete disappearance of the upward relaxation of Pt$_{(111)}$ atoms in the bottom layer that was found in ref 11, and hence, the bond length distribution and bond disorder changes. Essentially, the increased interlayer distances among Pt layers mean larger NN Pt−Pt bond lengths.

As listed in Table 2, the first NN Pt−Pt bond length increases from 2.68 Å without H passivation (e.g., in He) to 2.75 Å with H passivation. This 3% increase of Pt−Pt first NN bond length in Pt$_{37}$ due to passivation now agrees quantitatively well with experiments that perform an anneal in H$_2$ atmosphere before characterization.[16,20−24] We note that EXAFS measures an ensemble average but that the cluster size distribution found in experiment was narrow. Hence, the principle effect for increase

Table 2. Pt−Pt Bond Length and Coordination Number in Nearest-Neighbor (NN) Shells of Pt$_{37}$/C[a]

NN shell	bond length (Å)			coordination number	
	TC Pt$_{37}$ with H	TC Pt$_{37}$ without H	sheared Pt$_{37}$ without H	TC Pt$_{37}$ w/o H	sheared Pt$_{37}$ without H
1	2.75	2.68	2.67	6.97	6.76
2	3.90	3.72		2.43	
3	4.74	4.61		7.14	
4	5.43	5.25		3.24	

[a] With H, the shear instability is removed and bond lengths are increased in agreement with experiments (see text). See bond-length distribution in Figure 6. The sheared structure of Pt$_{37}$/C without H is shown in Figure 1b.

in NN bond length is not ensemble-average related but due to H passivation during processing. Indeed, for small Pt nanoparticles with first-shell coordination numbers around 6, recent EXAFS experiments[24] in H$_2$ and He atmosphere confirm the change in Pt−Pt first NN bond lengths, e.g., 2.75 Å with H$_2$ and 2.70 Å with He for Pt clusters supported on γ-alumina at 175 K. On a different kind of carbon support (i.e., carbon nanofibers), Koningberger et al.[23] has shown Pt−Pt bonds increase due to H (2.69 ± 0.2−2.76 ± 0.2 Å). Even though their Pt particles sit on a prismatic (instead of basal) plane of graphite, the H-induced effect on Pt−Pt bond is similar to ours. And, interestingly, our results show that extra H can easily go into the interface between Pt particle and carbon support. Pt−Pt bond lengths also increase in the higher shells as listed in Table 2.

We note that the H passivation effect on Pt−Pt bond length is strongly size-dependent. For smaller Pt nanoparticles with first-shell coordination numbers from 5 to 7, an increase of Pt−Pt bond length has been observed on various supports.[16,20−24] But for larger Pt nanoparticles with a coordination number beyond 8, no such effect has been observed. The reason is that the relation between first-shell coordination number and particle size is not linear, roughly proportional to the square root of the particle diameter. For example, the first shell coordination number for TC Pt$_{10}$, Pt$_{37}$, Pt$_{92}$ clusters, and bulk Pt are 4.80, 6.97, 8.20, and 12.0, respectively. A small increase in the coordination number above 8 can reflect a much larger cluster and substantially more bulk-like Pt bonds. Thus, the H passivation effect on Pt−Pt bond length should disappear rapidly for larger Pt particles.

As shown in Figure 6a, the first NN Pt−Pt bond length has a broad multi-modal distribution from 2.62 to 2.93 Å. The longest Pt−Pt bond is between the center of Pt(100) facet and
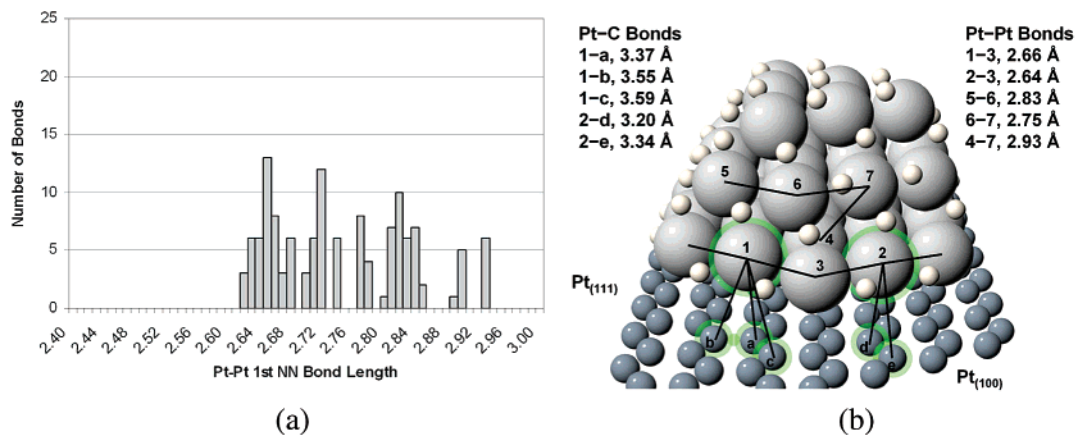
Figure 6. (a) For a TC−Pt$_{37}$/C passivated with 46 H, the distribution of NN Pt−Pt bond lengths, with average of 2.75 Å. The relaxed structure is shown in (b), with legend as in Figure 5. Significant Pt−C and Pt−Pt bonds (defined by the two connected atoms) are denoted by black line and corresponding bond lengths are listed. Pt and C are labeled in numbers and letters, respectively. Pt$_{(111)}$, Pt$_{(100)}$, and closet C atoms are highlighted.
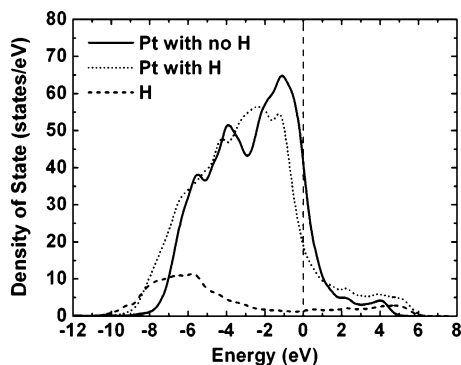

Figure 7. Projected density of states on Pt (with[out] H passivation solid [dotted]) and H (dashed) for a Pt$_{37}$/C. The Fermi level is energy zero (vertical dashed line). Stabilization via H adsorption is evident from the decrease of states at Fermi level with concomitant increased states at energy well below the Fermi level.

a Pt atom in the bottom layer (labeled 4−7). The shortest Pt−Pt bond is between two Pt atoms in the bottom layer (labeled 2−3). The highlighted Pt$_{(111)}$ and Pt$_{(100)}$ atoms (in green halos) are in the same plane as the other Pt in the bottom layer and the Pt−Pt bond lengths in the central layer perimeter are almost the same. This is in distinct contrast to the bare Pt$_{37}$/C where the central layer had successive long and short Pt−Pt bond around its perimeter leading to the much smaller bond lengths when cluster is annealed in helium.[11] Again the large Pt−C distances show that Pt−C interaction is very small.

Coordination Number and Morphology Change. Also listed in Table 2 are coordination numbers of the sheared structure that occur without H passivation, shown in Figure 1b, and those of the TC structure that occurs from H passivation. For the sheared structure, only the coordination number of the first shell is listed since the coordination numbers in the higher shells are not well defined. Compared with a TC structure, the sheared structure has only a 0.2 smaller first-shell coordination number. This small decrease agrees with our collaborators' recent EXAFS experiment on Pt nanoparticles on γ-Al$_2$O$_3$ (from 5.8 ± 0.2 with H passivation to 5.5 ± 0.2 without H passivation).[24]

We note that other EXAFS studies on Pt nanoparticles of similar size (with first shell coordination number of 5−7) on different supports also reported such small decreases in first-shell coordination number upon the removal of H passiva-

tion.[16,20] Unlike the morphology change found in our DFT calculations for Pt$_{37}$/C, which is due to the shear instability without H passivation, ref 20 concluded that there is no structural change of Pt nanoparticles with(out) H passivation. Even though the morphology change of supported Pt nanoparticles should be affected by the difference in metal−support as well as metal-adsorbate interaction, our results clearly show that small changes in the first-shell coordination number cannot rule out the possibility of a morphology change. Thus, the common assumption in EXAFS analysis that a small coordination number change implies that no morphological change has occurred should be verified case by case.

Electronic Structure and Origin of Bond Length Increase. In Figure 7, the electronic density of states (DOS) are projected on Pt and H in the H-passivated TC−Pt$_{37}$/C. The DOS projected on Pt in the unpassivated case is also shown. The Pt *d* bands and H *s* band hybridize to give bonding states starting from 10 eV to the Fermi level. The effect is to shift Pt-derived bands to lower energy, leaving the highest-energy antibonding states just above the Fermi level. This picture of hybridization between Pt *d* bands and H *s* band for the H-passivated Pt cluster is the same as that studied for the adsorption of hydrogen on semi-infinite Pt surfaces.[41] The bonding between Pt and H is at the cost of weakening the Pt−Pt bonding, which concomitantly increases the NN Pt−Pt bond lengths, as shown earlier. The antibonding states just above the Fermi level was suggested to be responsible for the shift of Pt L$_3$ white line in XANES.[16,18]

Conclusion

In conclusion, we have shown that hydrogen (H) passivation stabilize the truncated cuboctahedral structure of Pt$_{37}$ cluster supported on carbon by removing an electronically induced shear instability of Pt(001) facets−an effect responsible for the reconstruction of semi-infinite bulk Pt(001) surfaces. Without H passivation, the morphology change of the Pt$_{37}$ cluster is driven by the shearing of (100) to (111) facets to lower the surface energy, yet the change in the first-shell coordination is small (∼0.2) and, hence, cannot be used as an indication that there is no morphological change. With H passivation, the shearing is reversed by a much-preferred adsorption of H atom on the bridge sites of the (100) facets, which should be included in a realistic model of H adsorption on Pt nanoparticles. This structural reversal from sheared to unsheared cuboctahedral

morphology is downhill in energy, and leads to the observed truncated cuboctahedral structure for carbon-supported Pt nano-particles annealed in hydrogen atmosphere. Due to H passivation, the Pt−C interaction is reduced and the first nearest-neighbor Pt−Pt bond length is increased by 3%, which agrees quantitatively with EXAFS data.[16,20−24] Our results highlight the importance of considering the experimental processing and annealing conditions before directly comparing experimental and theoretical results, and reveal the nature of bulk-like structural instabilities that persist down to nanoscale clusters. All the physical changes result from a fundamental electronic effect—incomplete filling of Pt d states at the Fermi level, which is also why hydrogen is adsorbed readily and reverses the innate shear instability. These results should be particularly useful as a guide for interpreting experiments, such as EXAFS, where models must be generally considered, and again highlights the importance of passivation and morphological changes in the observed properties of nanoparticles.

JA068750H